AIR VELOCITY PROFILES AROUND THE HUMAN BODY

S.KW. Chang, Ph.D.

R.R. Gonzalez, Ph.D.
Member ASHRAE

ABSTRACT

The air velocity profiles around the human body were mapped at six selected sites—head, chest, upper arm, lower arm, thigh, and lower leg—using omnidirectional anemometers in an environmental chamber with precise airflow control. Two manikins, one standing and one sitting, were used to represent the anthropometric features and contour of the human body. We found that the air velocity profiles around each of the six sites displayed complex patterns. Furthermore, the profiles around the limbs were asymmetrical. The commonly used points of measuring the regional air velocities, such as the frontal stagnation and the right/left side streaming positions, were inadequate choices. Indeed, no single measurement position can be described as a good choice. The complex air velocity variations around the human body cannot be quantified by monitoring with a single anemometer. Only through elaborate mapping, such as the method employed in this study, can the air velocity profiles be described. The chamber's free stream air velocity did not match any of the regional air velocities. However, we did find that the free stream air velocity was an acceptable estimate of the overall whole body mean air velocity in both the standing and sitting manikin.

INTRODUCTION

Air velocity is one of the basic physical factors that defines the thermal environment and it is one of the main independent parameters that determines convective heat transfer and evaporative heat loss from the human skin (ISO 1985). In the heating, ventilating, and air-conditioning (HVAC) field, air velocity is a critical variable in the evaluation of the air diffusion performance index (ADPI) or the thermal comfort indices such as predicted mean vote (PMV) or predicted percentage of dissatisfied (PPD) (ISO 1984). Environmental chambers are often relied upon to provide the desired air velocity field. However, it has been found that the air velocity profiles of an environmental chamber could show large variations that can only be described with an elaborate multiple anemometer and multiple position mapping (Chang and Gonzalez 1991). This logically leads to the question of what is the air velocity profile encountered by a human body inside the chamber? Indeed, an equally relevant question might be how should the air velocity encountered by a shape as complex as the human body be measured?

Traditionally, air velocity encountered by a human body standing or sitting in the chamber is assumed to be uniform, and this uniform air velocity is represented by the chamber's free stream air velocity. When regional measurements are necessary, such as for specific regional convective heat transfer determination, a single frontal (Chang et al. 1988; Sogin 1958) or side position (Nishi and Gagge 1970) was used for each region. An initial set of air velocity data in Table 1 showed that neither the frontal nor the right-side air velocity resembled the chamber's free stream air velocity. The frontal site exhibited a stagnation point, and the right side a large streaming point. The questions raised above can only be answered by a careful mapping of the air velocity profile surrounding the human body inside an environmental chamber.

This paper reports an air velocity profile mapping technique for quantifying the profile around the human body in an environmental chamber with precise airflow control. Two human body postures, standing and sitting, were examined. The air velocities were measured at six selected body sites with omnidirectional anemometers. The air velocity profiles around the six sites were plotted to provide a visual representation of the variations in air velocity patterns.

METHOD

Air velocity profiles at six selected body sites—head, chest, upper arm, lower arm, thigh, and lower leg—were measured. The six body sites are depicted in Figures 1 and 2. Two life-size, unheated, stationary manikins were used to represent the human body posture while standing (see Figure 1) and sitting on a chair (see Figure 2). The standing manikin models a person 5 ft, 8 in. (1.72 m) in height. Both manikins have the same body surface area of 18.1 ft^2 (1.68 m^2). The manikins offered the anthropometric human body features and contour, and the advantage of absolutely reproducible postures. Data from the standing and the

Stephen KW. Chang is a research biomedical engineer and **Richard R. Gonzalez** is chief of the Biophysics and Biomedical Modeling Division, Environmental Physiology and Medicine Directorate, U.S. Army Research Institute of Environmental Medicine, Natick, MA.

TABLE 1
Frontal and Right-Side Air Velocity Measurement Comparison

Anemometer Position	UpArm	LoArm	Thigh	LoLeg
Frontal	1.06 mph (0.474 m/s)	1.71 mph (0.765 m/s)	1.46 mph (0.654 m/s)	1.49 mph (0.666 m/s)
Right Side	2.73 mph (1.22 m/s)	3.24 mph (1.45 m/s)	3.71 mph (1.66 m/s)	5.10 mph (2.28 m/s)

Chamber free stream air velocity 2.5 mph (1.12 m/s)

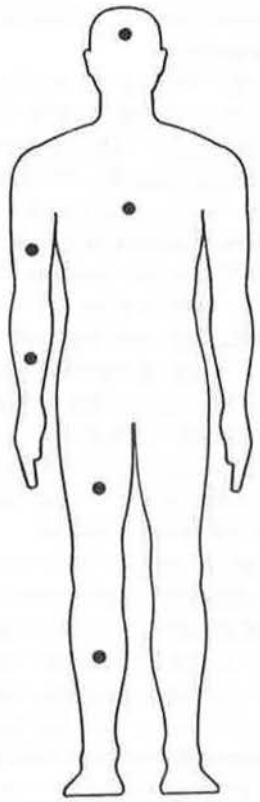

Figure 1 *Standing manikin.*

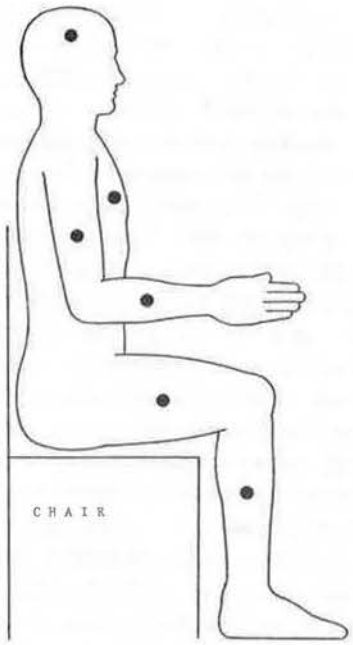

Figure 2 *Sitting manikin.*

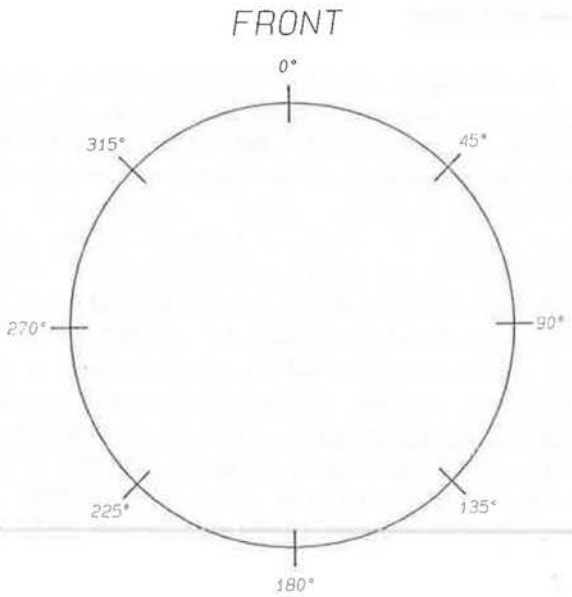

Figure 3 *Anemometer radial positions.*

sitting manikin were measured separately. At each measurement site, the anemometers were placed at eight radially spaced positions: 0° (front), 45°, 90° (right side), 135°, 180° (back), 225°, 270° (left side), and 315° (see Figure 3). For the standing manikin, all of the body limbs assumed a vertical orientation. For the sitting manikin, the limb segments of the lower arm and the thigh were in a horizontal orientation. For these horizontal limbs, the 0° position represents the top (rather than the front) of the sites, and the 180° position represents the area underneath (rather than the back of) the sites. At the chest site, for the 45° and 315° positions, the anemometer probes were placed above the pectoral muscle in the vicinity of the nipples. For the 135° and 225° positions, the probes were placed in the vicinity of the scapulae.

The six omnidirectional thermal anemometers were mounted on a telescoping tripod support (see Figure 4). The

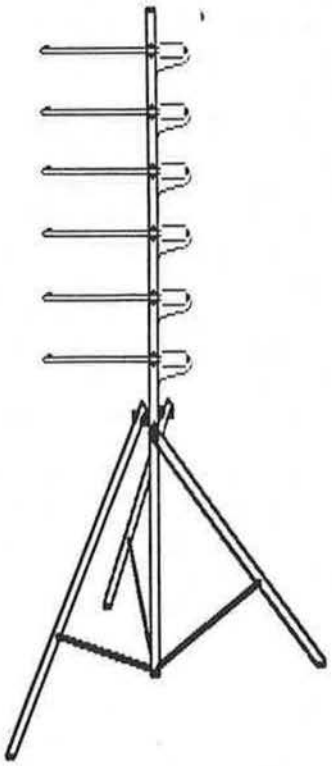

Figure 4 *Anemometer telescoping tripod support.*

air velocities were measured with the anemometer probe placed 0.39 in. (1.0 cm) from the designated body sites. As much as possible, the anemometer probes were oriented at a 90° angle to the direction of the chamber airflow to minimize the yaw angle and roll angle effects. The omnidirectional anemometer probes have a range between 0 and 600 fpm (0 and 3.00 m/s). The time constant of the anemometer is 2 seconds. The air velocity data were linearized with special hardware circuitry, fed through an analog-to-digital converter, and then collected using a desktop personal computer.

The environmental chamber employs aspirated airflow. The airstream flows from the front to the back of the chamber. At the airstream entrance, honeycomb-shaped grids are employed to minimize turbulence. The chamber dimensions are 15 ft × 11 ft × 8 ft (L × W × H). The manikins were placed an equal distance from the left and right walls, and 4.9 ft (1.5 m) from the back side of the chamber. The manikins faced the airflow frontally (i.e., head-on). Four chamber air velocity settings were used: 1 mph (0.447 m/s), 2 mph (0.894 m/s), 3 mph (1.34 m/s), and 4 mph (1.79 m/s). The chamber's free stream air velocity was measured with an independently calibrated thermal anemometer placed at a height of 67 in. (1.7 m) from the chamber floor and a distance of 87 in. (2.2 m) in front of the manikin. The anemometer was positioned to measure an unobstructed free stream. The chamber also has precise temperature and humidity control. The chamber temperature was set to 70°F (21°C), with relative humidity at 50%. The chamber was cleared of all articles except for the manikin and the data acquisition equipment. The data acquisition equipment was situated so as to minimize any interference of the airflow to the manikin.

At each chamber air velocity setting, one anemometer was placed at each body site, with all six at the same radial position. Air velocity data were collected at 3-second intervals for a continuous 10-minute period. After the 10-minute collection period, the chamber air velocity was changed to a different setting, and another round of 10-minute data collection was initiated. The order of chamber air velocity setting was randomly determined. After all four chamber air velocities had been used, the six probes were then moved to the next radial position to begin another four rounds of 10-minute data collection (one for each chamber air velocity setting). This process continued until all eight radial positions were completed. Therefore, each complete set of data contained four rounds of measurement, with each round composed of data from all six body sites at eight probe positions.

Additional data were collected from a sphere-and-cylinder setup (Figure 5). Because the manikin's regional air velocities were found to be quite asymmetrical, the sphere-and-cylinder setup was used to ensure that the data asymmetry was a real effect and not a result of orientation

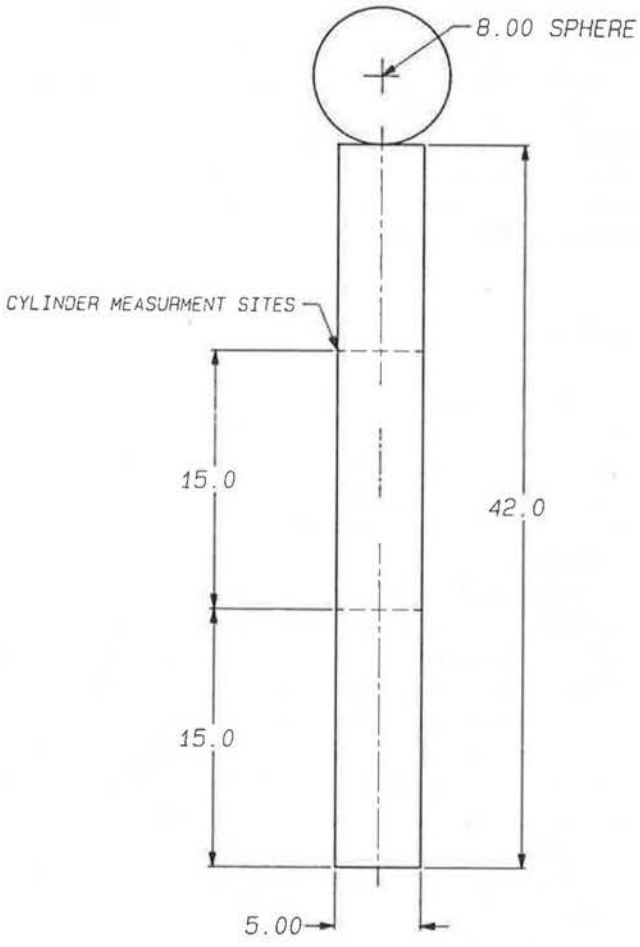

Figure 5 *Sphere-and-cylinder setup.*

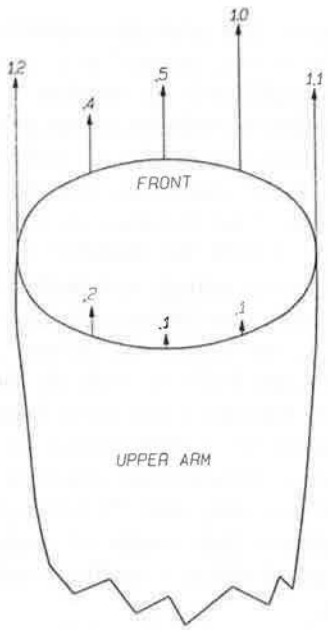

Figure 6 *Three-dimensional representation of the air velocity profile numbers indicating air velocity magnitude.*

error or other unknown omnidirectional anemometer anomalies. The sphere-and-cylinder configuration should yield symmetrical air velocity plots. The cylinder air velocity profiles serve as a comparison baseline for the limb data, as the manikin's limbs can be approximated as cylinders. The sphere data serve as a comparison baseline for the manikin's head, which can be approximated as having a spherical shape. The sphere has a diameter of 8 in. The cylinder has a diameter of 5 in. and a height of 42 in. Air velocities around the sphere and around two sites on the cylinder were measured. The sites are shown in Figure 5.

RESULTS

A total of nine data sets from the standing manikin and six data sets from the sitting manikin were collected. In addition, four sets of data were collected from the sphere-and-cylinder setup. Plots of the measured air velocity profiles were developed to aid in the visualization of the air velocity patterns.

One choice of visual representation would be a simulated three-dimensional view, as in Figure 6, where higher air velocities are represented as longer arrows pointing upward. However, as is evident in Figure 6, this three-dimensional method does not allow the shape of the air velocity profile to be easily visualized. Another disadvantage of the three-dimensional representation is that plots from the four chamber air velocity settings cannot be presented together, using common axes, for comparison.

The method of representation used in this report is a two-dimensional profile, where higher air velocities are represented radially outward from the center, as in Figures 7 through 14. The body sites are shown as a circle in the center of the plot (except for the chest site), representing a cross-sectional top view of the body segment. For the horizontal body segments of the sitting manikin, as described earlier, the cross-sectional views represent a back view, i.e., looking toward the front from the back of the manikin. For the chest site, elliptical plots were used to approximate the cross-sectional top view of the main body trunk. In Figures 7 through 14, four symbols represent air velocity data measured at each of the four chamber settings: 1 mph, ○; 2 mph, Δ; 3 mph, □; and 4 mph, ∇. On the radial (polar) plots, each unit represents 0.224 mph (0.10 m/s). The curves that connect the eight data points around each body segment were only used to aid visualization. The curves do not represent continuous data points.

The mean data from entire data sets were used in the plots for each manikin, body site, and probe position. Figures 7 and 8 were plotted from the sphere-and-cylinder data. Figures 9 through 14 are, respectively, the head, chest, upper arm, lower arm, thigh, and lower leg data from the standing (a) and sitting (b) manikin.

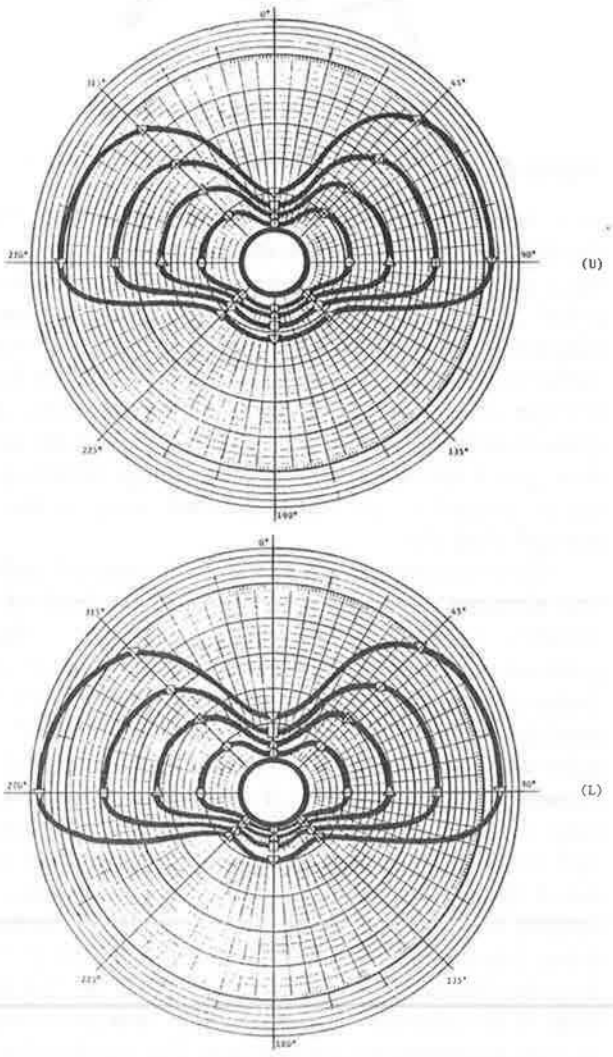

Figure 7 *Upper cylinder (U) and lower cylinder (L) air velocity profiles.*

DISCUSSION

Sphere-and-Cylinder

The upper cylinder and lower cylinder data in Figure 7 were essentially the same. Both were symmetrical about the sagittal midplane of the cylinder. The air velocity profile plots showed two distinct lobes, producing a "butterfly" shape. The frontal (0°) and the backside (135°, 180°, 225°) positions were stagnation points. High air velocities were measured at the expected streaming right and left sides (90° and 270° positions) and to a lesser extent at the 45° and 315° positions.

The air velocity profile of the sphere was also symmetrical (Figure 8); the lobes were more circular in appearance than in the cylinder case. There appeared to be only one stagnation point at the 0° position. In general, the backside produced no stagnation point. The regional air velocities were unexpectedly high. Different anemometers were used, and all gave readings in the same range.

The implication of the complex air velocity profiles around the sphere and the cylinder is that only through elaborate mapping, such as the method employed in this study, can the air velocity variations be understood. The two most often used positions, the 0° (frontal) and the 90°/270° (right side/left side) positions, are not good candidates for measuring the local site air velocity. The 0° position is, in general, a stagnation point and thus will give a low air velocity reading. The 90°/270° positions are streaming points and thus are expected to give very high air velocity readings. Indeed, no single anemometer monitoring will suffice in giving us any indication of the air velocity patterns that were found around the human body.

In Table 2, for each measuring site, data from the eight radially positioned probes were averaged to produced a site mean. As expected, comparison of Table 2 and Figures 7 and 8 found no obvious relationship between the site means and the regional air velocities around the sphere and the cylinder. The site means also did not agree with the chamber's free stream air velocities. No systemic method can be found for either using the site mean to derive the regional air velocities or vice versa, i.e., using any single regional air velocity to predict the site mean.

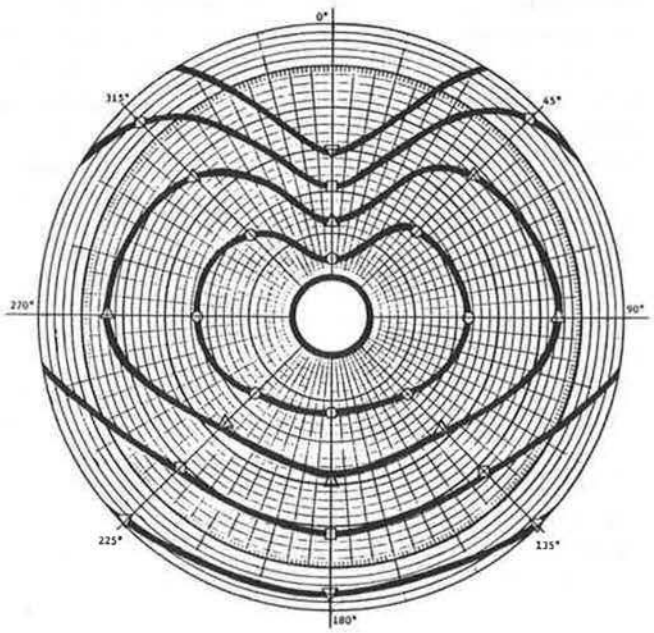

Figure 8 *Sphere air velocity profiles.*

Standing Manikin

The characteristic butterfly shape profile exhibited by the cylinder was, in general, not evident in the limb data of the standing manikin. All of the limb data in Figures 11a, 12a, 13a, and 14a were asymmetrical, reflecting the complex shape of the human body. The body trunk at the left side of the limb interfered with the airflow, resulting in low air velocity at the 315° position. In contrast, the absence of the body trunk to the right side of the limb resulted in air velocity at the 45° that was comparable to the 90° position, producing a profile similar to the cylinder data. This is illustrated most clearly at the lower leg site (Figure 14a), where the air velocity profile appeared as one-half the cylinder butterfly profile, i.e., without the left-side lobe.

The airflow around the complex body shape produced some interesting switching between stagnation and in-stream points. For the upper arm (Figure 11a), the backside positions (135°, 180°, 225°) first began as stagnation points. As the air velocity increased, the airflow gradually

TABLE 2
Sphere-and-Cylinder Site Averaged Air Velocities (m/s)

Chamber Free Stream	Sphere	Upper Cylinder	Lower Cylinder
1 mph (0.447 m/s)	0.821	0.334	0.283
2 mph (0.894 m/s)	1.63	0.642	0.610
3 mph (1.34 m/s)	2.42*	1.03	1.02
4 mph (1.79 m/s)	3.29*	1.51	1.54

* Some regional air velocities exceeded the maximum range of the omnidirectional anemometer, these means were estimated.

engulfed these positions. They switched from stagnation to in-stream points. The reverse phenomenon occurred at the head site (Figure 9a). The air velocity patterns at the 180° position were similar to the sphere data for chamber air velocity settings up to 3 mph. However, as the chamber air velocity increased further to 4 mph, the airflow became sufficiently large and left the anemometer probe in a stagnation pool. This position switched to a stagnation point, as the air velocity profile clearly showed.

For the standing manikin, site means (see Table 3) also were not informative about the air velocity variations around the sites, as in the sphere-and-cylinder case. Interestingly for the standing manikin, the chamber's free stream air velocity did appear to approximate the overall whole body mean air velocity rather well. The overall whole body mean was averaged from the six individual site means, with equal weight assigned to all six sites. A weighted mean was also computed in Table 3. The weights were adopted from the ratios of limb surface area to the total body surface area (Nishi and Gagge 1970). The weights used were: upper arm, 8%; lower arm, 9%; thigh, 20%; lower leg, 20%; chest, 35%; and head, 8%. The weighted mean contained a disproportionately large contribution from the chest air velocity data, because the large body trunk area is attributed to the chest site entirely. Nevertheless, the weighted mean agreed with the overall (equal weight) mean. The chamber's free stream air velocity proved to be an adequate approximation of both whole body mean data.

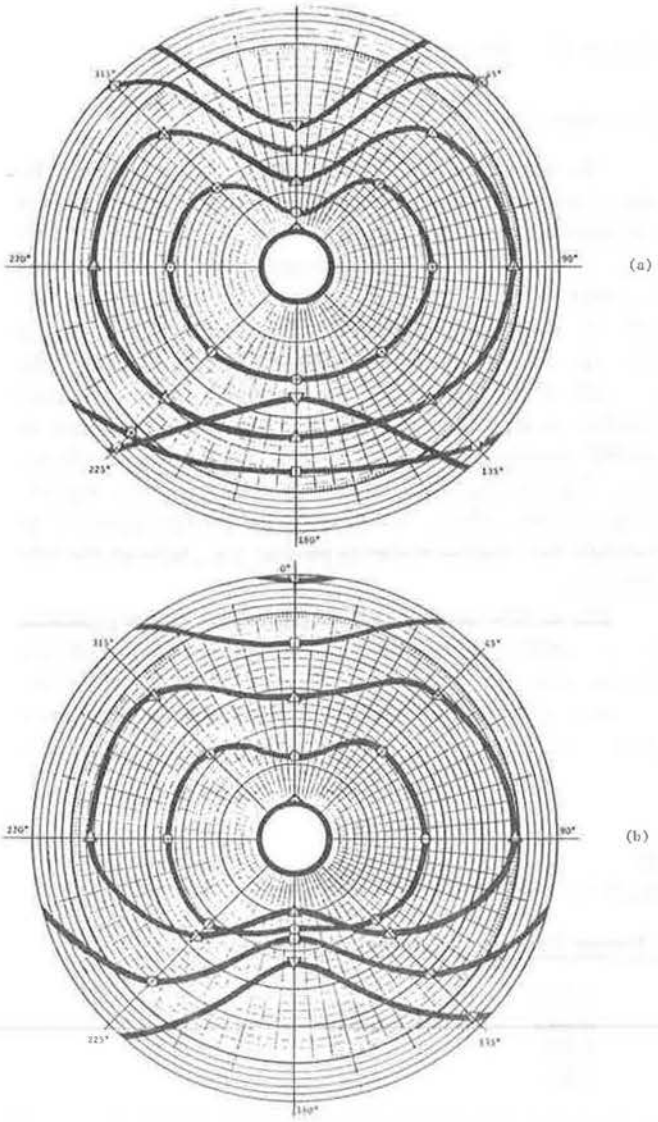

Figure 9 *Head air velocity profiles.*

Sitting Manikin

For the vertically oriented limb segments, the upper arm air velocity profile was less affected by body posture than that of the lower leg. Upper arm profiles of the standing and sitting manikins were similar (Figures 11a and 11b). The sitting lower leg profiles (Figure 14b) appeared quite different from the standing lower leg profiles (Figure 14a). The stagnation in Figure 14b seemed less prominent at the usual sitting posture stagnation points of 135°, 180°, 225°, and 315°. This could be the result of interference or interaction with the chair.

The chest profiles of the standing and sitting manikins were quite similar (Figures 10a and 10b). Some differences were found between the head air velocity profiles (Figures 9a and 9b). In the standing manikin, 0° (front) position was a stagnation point, whereas the 180° (back) position was in

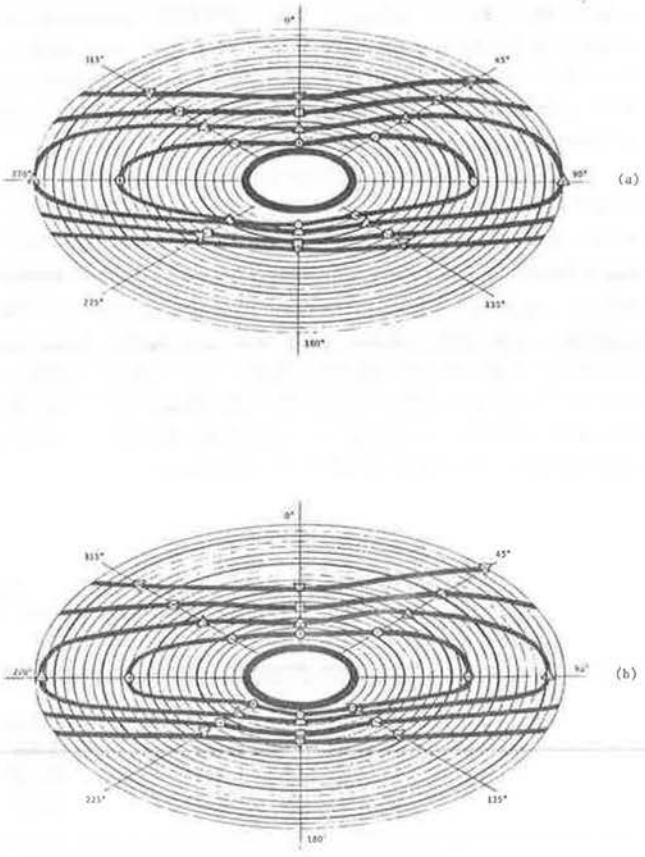

Figure 10 *Chest air velocity profiles.*

TABLE 3
Standing Manikin Site and Whole Body Mean Air Velocities

STANDING MANIKIN (air velocity in m/s)

Chamber Free Stream	Head	Chest	UpArm	LoArm	Thigh	LoLeg	Overall Mean	Weighted Mean
1 mph (0.447 m/s)	1.01	0.570	0.270	0.355	0.423	0.184	0.468	0.455
2 mph (0.894 m/s)	1.89	1.01	0.585	0.782	0.815	0.405	0.914	0.864
3 mph (1.34 m/s)	2.70*	1.48*	1.07	1.30	1.36	0.696	1.43*	1.35*
4 mph (1.79 m/s)	3.17*	2.00*	1.84	1.80*	1.86*	1.18	1.98*	1.87*

* Some regional air velocities exceeded the maximum range of the omnidirectional anemometer, these means were estimated.

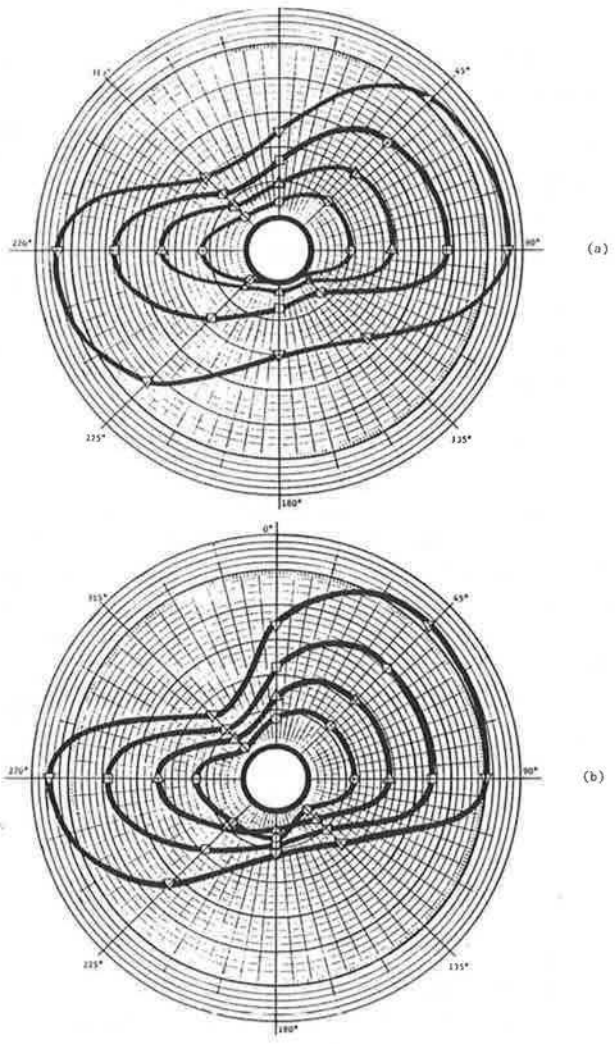

Figure 11 *Upper arm air velocity profiles.*

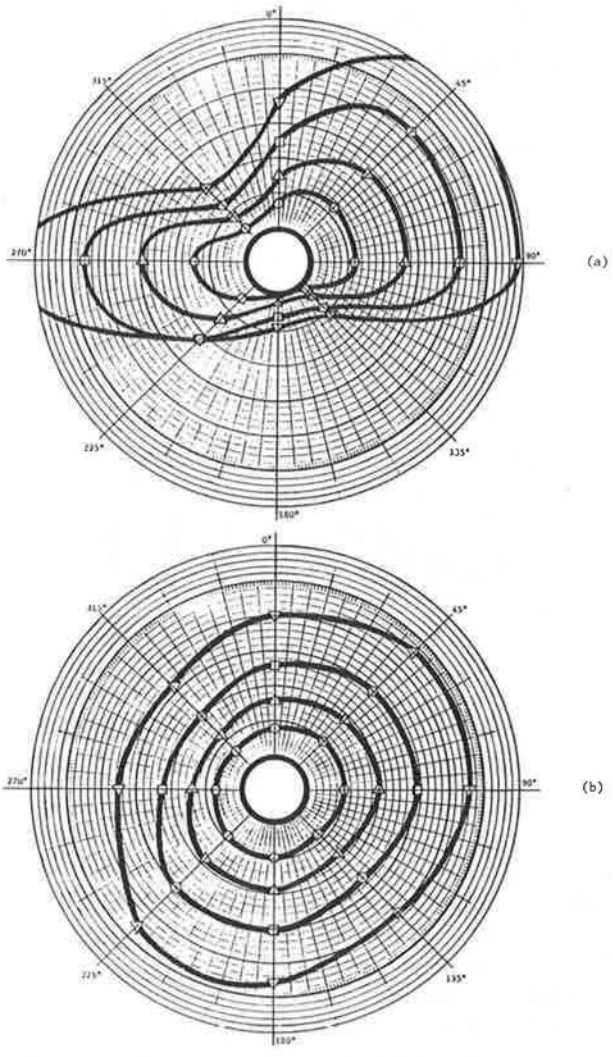

Figure 12 *Lower arm air velocity profiles.*

TABLE 4
Sitting Manikin Site and Whole Body Mean Air Velocities

SITTING MANIKIN (air velocity in m/s)

Chamber Free Stream	Head	Chest	UpArm	LoArm	Thigh	LoLeg	Overall Mean	Weighted Mean
1 mph (0.447 m/s)	1.02	0.510	0.414	0.422	0.340	0.205	0.486	0.440
2 mph (0.894 m/s)	1.68	0.915	0.694	0.838	0.730	0.475	0.888	0.826
3 mph (1.34 m/s)	2.52*	1.42*	1.12	1.36	1.15	0.838	1.40*	1.31*
4 mph (1.79 m/s)	3.44*	1.97*	1.69	2.09	1.69	1.41	2.05*	1.91*

* Some regional air velocities exceeded the maximum range of the omnidirectional anemometer, these means were estimated.

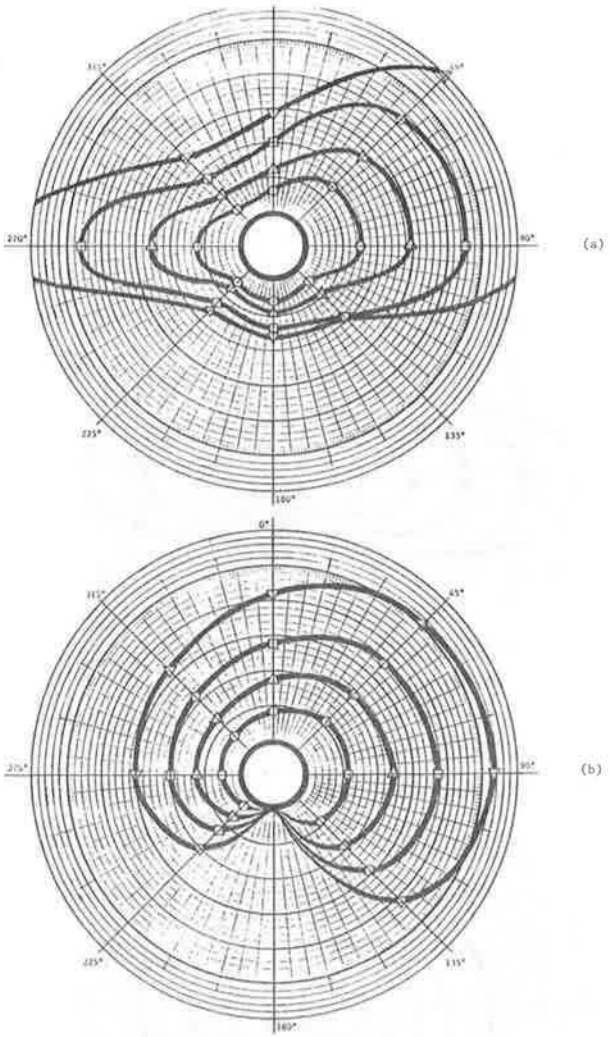

Figure 13 Thigh air velocity profiles.

general not stagnant. For the sitting manikin, the situation was reversed. The 0° position was not stagnant, while the 180° showed as a stagnation point. The reason for this difference was not apparent.

The most prominent difference between the standing and sitting manikins occurred at the lower arm and thigh (Figures 12 and 13). These two limb segments were vertical in the standing posture but assumed a horizontal orientation in the sitting posture. The air velocity profiles of the lower arm (Figure 12b) were nearly circular, with equal magnitude around the limb. The deviation from a perfect circular shape could be the result of interaction of the hand with the airflow. The thigh profiles (Figure 13b) were more asymmetrical. The body trunk obviously interfered with the left-side airflow. Also for the thigh, the 180° (underneath) position was in contact with the chair, thus no air velocity was measured.

Site means, overall whole body (equal weight) mean, and weighted mean were also computed for the sitting manikin in Table 4. Similar conclusions can be drawn for both the standing and sitting manikins. No relationship can be found between site means and the site regional air velocities. Again, the overall whole body mean air velocity and the weighted mean were in general agreement. Both whole body means can be estimated by the chamber's free stream air velocity.

Free Stream Air Velocity

The reason that the chamber's free stream air velocity should approximate the whole body mean air velocity for both the standing and the sitting manikins is not directly apparent. Perhaps the fact that both manikins have the same total body surface area is an important factor. Rapp (1973) did find that the convection of a standing, sitting, and reclining nude man can be rationally and very uniquely modeled by a sphere having the same Dubois surface area as that of the nude man. This free stream air velocity result may be puzzling but also fortuitous. By knowing only the chamber's free stream air velocity, we can apparently obtain good estimation of quantities that are attributable to the entire body, such as the whole body convective heat transfer.

Whole body predictive indices such as the thermal comfort PMV and PPD are calculated using a single air velocity value. Usually, the free stream air velocity is used. The result of this study appears to justify the free stream air velocity as an adequate choice for the whole body index

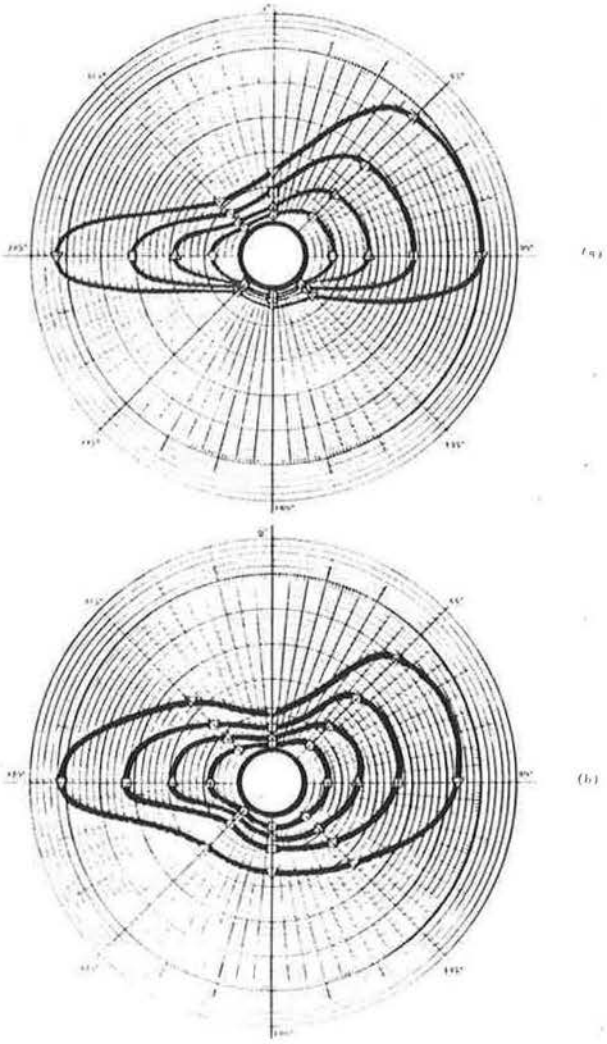

Figure 14 *Lower leg air velocity profiles.*

calculation. However, the asymmetrical regional air velocities found in this study undoubtedly will also affect human thermal comfort votes. Within an asymmetrical thermal environment, it is possible to feel localized discomfort while the whole body is thermally neutral (Gonzalez 1983). As the thermal comfort index is presently formulated, no mechanism is available to accommodate any possible localized discomfort.

CONCLUSION

Air velocity profile mapping around the human body using multiple anemometers indicated such profiles were very complex and in general asymmetrical. The complexity cannot be quantified or predicted by customary monitoring using a single anemometer. The complex profiles can only be understood through an elaborate multiple anemometer and multiple position mapping, such as the method described in this study.

We also found that the chamber's free stream air velocity appeared to estimate the whole body mean air velocity for both the standing and the sitting manikin data. The reason is not precisely known. The result presents a curious situation in that the free stream air velocity will allow us to estimate parameters affecting the whole body, such as the whole body convective heat transfer, even though we do not know anything about the regional air velocities. This result is certainly fortuitous, since the commonly, although erroneously, made assumption is that the air velocity around a human body inside a chamber is uniform and the uniform air velocity is taken as the chamber's free stream air velocity.

REFERENCES

Chang, S.KW., and R.R. Gonzalez. 1991. Air velocity mapping of environmental test chambers. *ASHRAE Transactions* 97(1): 31-36.

Chang, S.KW., E. Arens, and R.R. Gonzalez. 1988. Determination of the effect of walking on the forced convective heat transfer coefficient using an articulated manikin. *ASHRAE Transactions* 94(1): 71-82.

Gonzalez, R.R. 1983. Infrared radiation and human thermal comfort. In *Microwaves and Thermoregulation*, E. Adair, ed., pp. 109-137. New York: Academic Press.

ISO. 1984. *ISO International Standard 7730, Moderate thermal environments—Determination of the PMV and PPD indices and specification of the conditions for thermal comfort*. Geneva: International Organization for Standardization.

ISO. 1985. International Standard 7726, Thermal environments—Instruments and methods for measuring physical quantities. Geneva: International Organization for Standardization.

Nishi, Y., and A.P. Gagge. 1970. Direct evaluation of convective heat transfer coefficient by naphthalene sublimation. *Journal of Applied Physiology* 29: 803-838.

Rapp, G.M. 1973. Convective heat transfer and convective coefficients of nude man, cylinders and spheres at low air velocity. *ASHRAE Transactions* 79(1): 75-87.

Sogin, H.H. 1958. Sublimation from disks to air streams flowing normal to their surfaces. *Transactions ASME* 80: 61-69.